Corrosion Behavior of Carbon Steel at Typical Positions of an Amine-Based CO2 Capture Pilot Plant

ARTICLE *in* INDUSTRIAL & ENGINEERING CHEMISTRY RESEARCH · MAY 2012

Impact Factor: 2.59 · DOI: 10.1021/ie203045v

5 AUTHORS, INCLUDING:

Jubao Gao
Chinese Academy of Sciences
13 PUBLICATIONS **60** CITATIONS
SEE PROFILE

Shujuan Wang
Tsinghua University
72 PUBLICATIONS **539** CITATIONS
SEE PROFILE

Bo Zhao
Tsinghua University
30 PUBLICATIONS **212** CITATIONS
SEE PROFILE

I&EC research
Industrial & Engineering Chemistry Research

Article

pubs.acs.org/IECR

Corrosion Behavior of Carbon Steel at Typical Positions of an Amine-Based CO_2 Capture Pilot Plant

Jubao Gao, Shujuan Wang, Chenchen Sun, Bo Zhao, and Changhe Chen

Key Laboratory for Thermal Science and Power Engineering of Ministry of Education Department of Thermal Engineering, Tsinghua University, Beijing 100084, People's Republic of China

ABSTRACT: Corrosion tests of carbon steel at six typical positions in a CO_2 capture pilot plant using amine-based solvent were conducted with simulated flue gas (12 vol % CO_2, 18 vol % O_2 and 214 ppm SO_2). A weight-loss method was used to determine the corrosion rates for about 400 h of experiment. Scanning electron microscopy and energy dispersive X-ray spectroscopy were used to analyze the morphology and compositions of the coupon surface and cross section. The corrosion products on the sample's surface and cross section were analyzed with X-ray diffraction and Raman spectroscopy, respectively. Experimental and theoretical analyses show that the higher corrosion rates among these positions were present at the bottom of the absorber and rich liquid outlet of the rich-lean heat exchanger. The double-layer structure of the corrosion products with different colors was obviously observed on the cross sectional surface of the coupons at the absorber bottom and the stripper inlet. The corrosion products in the inner layer are mainly composed of hematite (α-Fe_2O_3) and magnetite (Fe_3O_4) with traces of goethite (α-FeOOH), while the outer layer mainly consists of siderite ($FeCO_3$). The inner corrosion products, including α-Fe_2O_3, Fe_3O_4, and α-FeOOH, may come from the decomposition of $FeCO_3$ in the amine-H_2O–CO_2–O_2–SO_2 system. An addition of SO_2 yields large amounts of hydrogen ion and dissolved oxygen which may induce a higher corrosion rate.

1. INTRODUCTION

Amine scrubbing systems have been used to separate CO_2 from natural gas in the chemical industry for several decades. It is still as timely solution to control global warming and climate change compared to other advanced technology.[1,2] However, the material corrosion creates unsafety and unreliability in the CO_2 capture system, which directly affects the whole system economics for solvents losses, unplanned downtime, reduced equipment life, and even injury.[3]

More useful information on corrosion in a CO_2 separation process using an amine-based absorbent was provided by some literature. Veawab et al. studied the influence of process parameters, including amine concentration, solution temperature, solution velocity, heat stable salt concentration, CO_2 loading and oxygen content, on corrosion behavior in single amine systems as well as mixed amine systems.[4−8] The corrosiveness increases with increasing amine concentration, solution temperature, solution velocity, heat stable salts, CO_2 loading, and oxygen content. Corrosion inhibitors, such as sodium sulfite (Na_2SO_3), sodium metavanadate ($NaVO_3$), carboxylic acid, and sulfoxide were also tested in an AMP-CO_2 system and an MEA-CO_2 system.[9,10] Their inhibition performances depended on the temperature and the inhibitor's concentration. The effect of SO_2 in the range of 0−204 ppm on corrosion of carbon steel in the CO_2 capture process was reported by Kladkaew.[11] It also leads to a higher corrosion rate. Corrosion product layers of carbon steel were investigated in CO_2-saturated MDEA solutions under 4.5 MPa CO_2 at 100 °C by Guo and Tomoe.[12] The corrosion product $FeCO_3$ followed by trace Fe_3O_4/$Fe(OH)_2$ was detected. The corrosion rates of steel at typical locations in two CO_2 capture pilot plants based on MEA were monitored using weight loss coupons and corrosometer probes.[13]

In this work, corrosion characteristics of carbon steel at typical locations in an amine based CO_2 capture pilot plant were analyzed, including corrosion rate, corrosion morphologies and corrosion products, with the aid of the weight loss method, scanning electron microscopy (SEM), energy dispersive X-ray spectroscopy (EDX), X-ray diffraction (XRD), and Raman spectroscopy. The study can help us to understand the CO_2 corrosion phenomena and mechanisms in mixed amine-H_2O–CO_2–O_2–SO_2 system.

2. EXPERIMENTAL SECTION

2.1. Materials. The N_2, O_2, CO_2, and SO_2 with more than 99.9% concentration were used to simulate flue gas. The chemical reagents were industrial grade, and the concentration was more than 98%. The blended amine solvent specified by Toshiba was used for this research work.

Coupons and coupon holders shown as Figure 1 were used for corrosion tests. Coupon holders were machined from AISI

Figure 1. Coupon holders and coupons for corrosion test.

Received: December 27, 2011
Revised: April 10, 2012
Accepted: April 11, 2012
Published: April 11, 2012

Table 1. Carbon Steel Chemical Composition

element	C	Si	P	S	Mn	Mo	N	Cr	Ni	Fe
weight (%)	0.053	0.031	0.016	0.034	0.25	/	/	0.025	0.012	balance

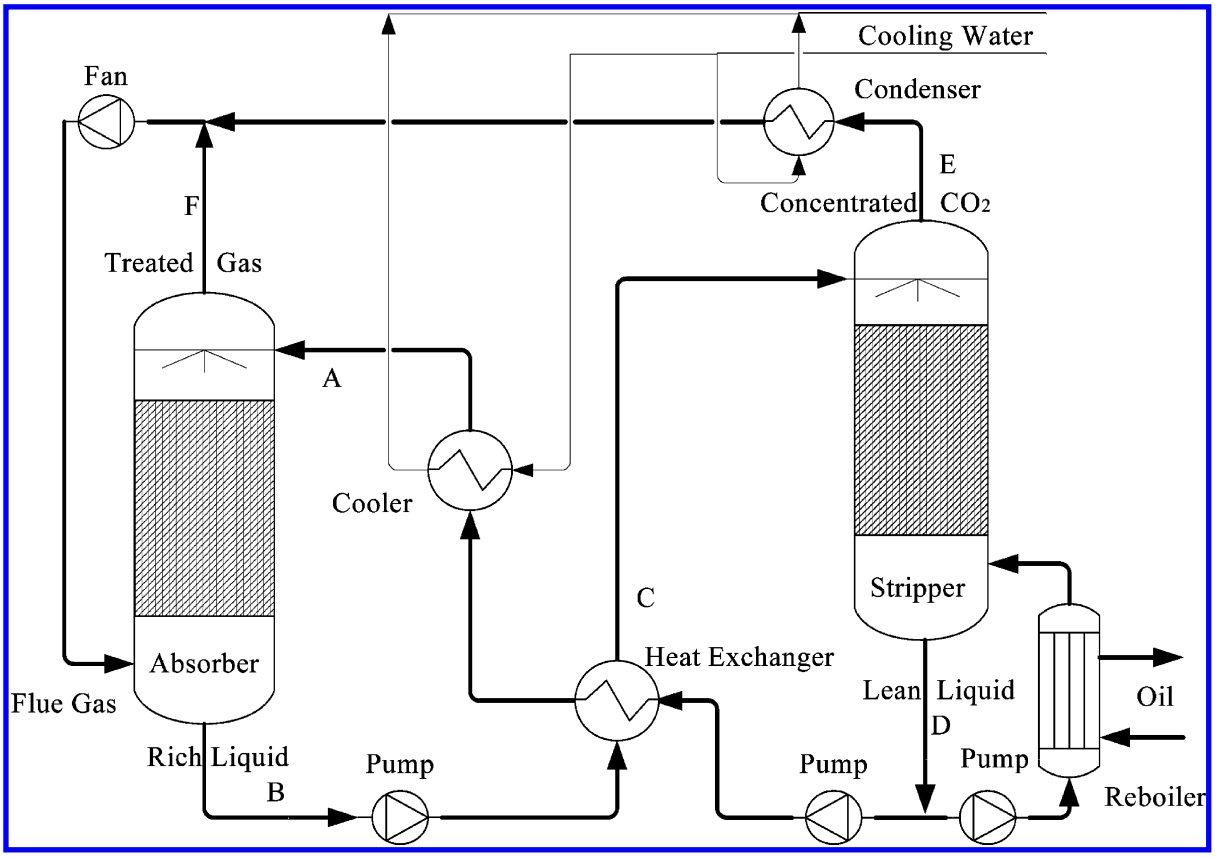

Figure 2. Flow diagram of experimental system and typical positions for corrosion test.

Table 2. Conditions of Different Positions

position	CO_2 content	amine concentration (mol/L)	T (°C)	flow rate (m/s)
A	0.05 mol/mol	4.34	45	0.33
B	0.16 mol/mol	4.34	48	0.09
C	0.16 mol/mol	4.34	101	0.32
D	0.05 mol/mol	4.34	116	0.84
E	99%		103	1.08
F	3.19%		43	11.51

304 stainless steel. The test specimens were made of carbon steel with size of 25 × 10 × 2 mm and 40 × 10 × 2 mm for different positions. PTFE gaskets were used to avoid electrochemical corrosion between coupon (carbon steel) and coupon holder (stainless steel). The detailed chemical composition of the carbon steel is shown in Table 1.

2.2. Analysis Methods. The corrosion rates were determined from the weight-loss method. The corrosion rate (R) can be calculated using the following equation:

$$R = \frac{8.76 \times 10^7 \times (M - M_1)}{\mathrm{STD}} \quad (1)$$

Where M, M_1, S, T, and D denote weight before reaction (g), weight after reaction (g), sample area (cm^2), reaction time (h), and sample density (kg/m^3), respectively.

The morphology and surface compositions of corroded coupons were analyzed with SEM, EDX (JSM-6301F), and XRD (D/max-2500). The cross sections of corroded coupons were analyzed with Raman spectroscopy (RM2000).

2.3. Experimental Procedure. Coupons were first polished and ground with 120- or 150-grit water abrasive paper, then degreased with magnesia and acetone, rinsed with alcohol at least three times, dried, weighed with a precision of 0.01 mg, and measured the surface area. After that they were installed at six different typical positions in the CO_2 capture pilot plant shown in Figure 2, including lean liquid inlet of absorber (A), rich liquid outlet of absorber (B), rich liquid inlet of stripper (C), lean liquid outlet of stripper (D), top of stripper (E), and top of absorber (F). After the test, the microstructure and compositions of coupons were examined. The weight of specimens was measured after removing the corrosion products. The operation was based on the Chinese standard JB/T7901−1999 named metals materials-uniform corrosion method of laboratory immersion testing.

dx.doi.org/10.1021/ie203045v | Ind. Eng. Chem. Res. 2012, 51, 6714−6721

The pilot plant is same as conventional amine-based CO_2 recovery plant except for recycled flue gas. The campaign was run for about 400 h with a feed gas of 12 vol % CO_2, 18 vol % O_2, 214 ppm SO_2, and N_2 as the balance. O_2 and SO_2 were continuously supplied. The average flue gas flow rate in the campaign was about 86 N m^3/h, and the average liquid solvent flow rate was around 0.6 m^3/h. The heat input to the stripper is supplied by an electrical heater with the maximum power of 60 kW. No fresh solvent and water was added into the system during the campaign. The main parameters at six typical positions are shown in Table 2. More details can be found in the literature.[14−16]

3. RESULTS AND DISCUSSION

3.1. Weight-Loss Tests. Figure 3 shows the corrosion rates of carbon steel at six typical positions. Many factors shown in

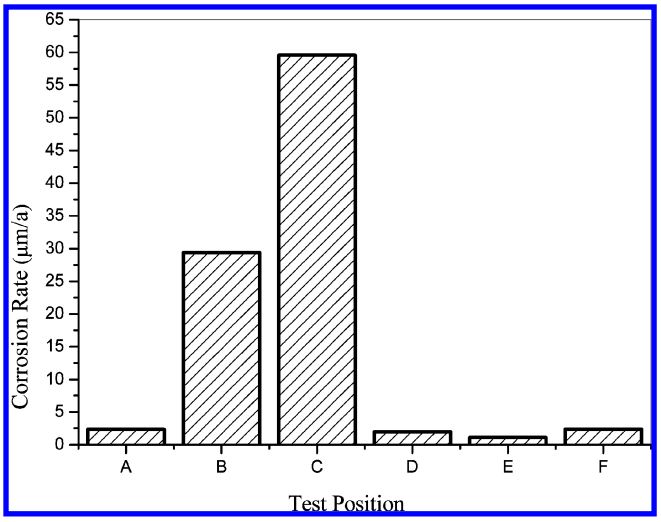

Figure 3. Corrosion rates at different positions.

Table 2, such as temperature, velocity, and CO_2 loading, are important process parameters influencing the corrosion rate. As to the absorbent inlet (A) and outlet (B) of the absorber, temperature was almost identical. The velocity at B was lower than that at A, which would lead to lower corrosion rate at B.[7] The corrosion rate at the rich liquid outlet (B), however, is much higher than that at A, as shown in Figure 3, which should be caused by the higher CO_2 loading. Such corrosion behavior caused by CO_2 loading could be simply explained with the following reactions.

Absorption of CO_2:

$$CO_2 + RNH_2 + H_2O \leftrightarrow RNH_3^+ + HCO_3^- \quad (2)$$

Possible cathodic reactions:[17]

$$2HCO_3^- + 2e^- \leftrightarrow 2CO_3^{2-} + H_2 \quad (3)$$

$$2H_3O^+ + 2e^- \leftrightarrow H_2 + 2H_2O \quad (4)$$

$$2H_2O + 2e^- \leftrightarrow H_2 + 2OH^- \quad (5)$$

$$O_2 + 2H_2O + 4e^- \leftrightarrow 4OH^- \quad (6)$$

Main anodic reaction:

$$Fe \rightarrow Fe^{2+} + 2e^- \quad (7)$$

where RNH_2 = amine, RNH_3^+ = protonated amine. Increase in CO_2 loading yields large amounts of RNH_3^+ and HCO_3^- which in turn produce more H^+, as shown in Figure 4, which

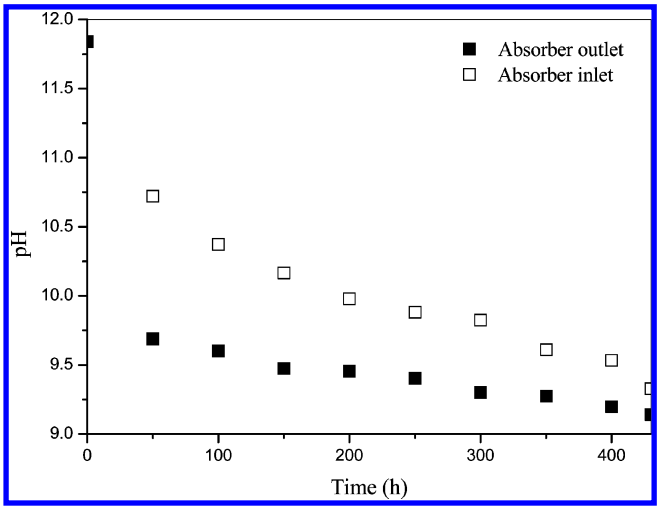

Figure 4. Solvent pH in the absorber at 298 K.

accelerates the cathodic reactions. This result is in good agreement with previous work by Veawab et al.[4−7] The same result can be concluded in the stripper. Although position D shows higher temperature and flow rate than C, the lower CO_2 loading induces the smaller corrosion rate. Therefore, the CO_2 loading is the main factor influencing the corrosion rate among the three parameters considered.

The corrosion rate at position C is the highest among six positions. Its higher temperature and velocity than that of B should be the main reason. Furthermore, a phenomenon of two phase flow was detected during the experiment, which may be caused by high temperature and CO_2 loading. At the beginning, the flow was transferred from firmness to instability. The intermittent slug flow was observed, and the solution flow rate was fluctuated. After that, the lacteal flow was detected, but the flow was relatively steady. Two-phase flow induces more serious corrosiveness than single phase flow because of the increased transport of both corrosion products and reactants.[18]

The flow medium is in the gas phase at positions E and F, which is different compared to others. Although the temperature and CO_2 volume percent at position E is higher than that at position F, the latter has a larger corrosion rate. The main reason may be the presence of free water and oxygen at position F, which is the main cathodic reaction. Meanwhile, the higher flow rate may be another reason to accelerate the corrosion product dissociation, and then result in a higher corrosion rate.

3.2. SEM Analysis Results. Figure 5 shows the surface morphologies of the six corroded coupons after about 400 h of prolonged operation. The polishing marks and small scattered compounds can be distinctly found in Figure 5A. However, when CO_2 loading increased from positions A to B (Figure 5B), the surface was locally covered with more loose corrosion products. And the presence of holes will result in further corrosion reaction. It can be seen from Figure 5C that the surface morphologies are almost identical and the compact crystalline particles were produced on the corroded surface. The corrosion products are shaped in a regular structure. These compounds were proven to be siderite by XRD. The surface

dx.doi.org/10.1021/ie203045v | Ind. Eng. Chem. Res. 2012, 51, 6714−6721

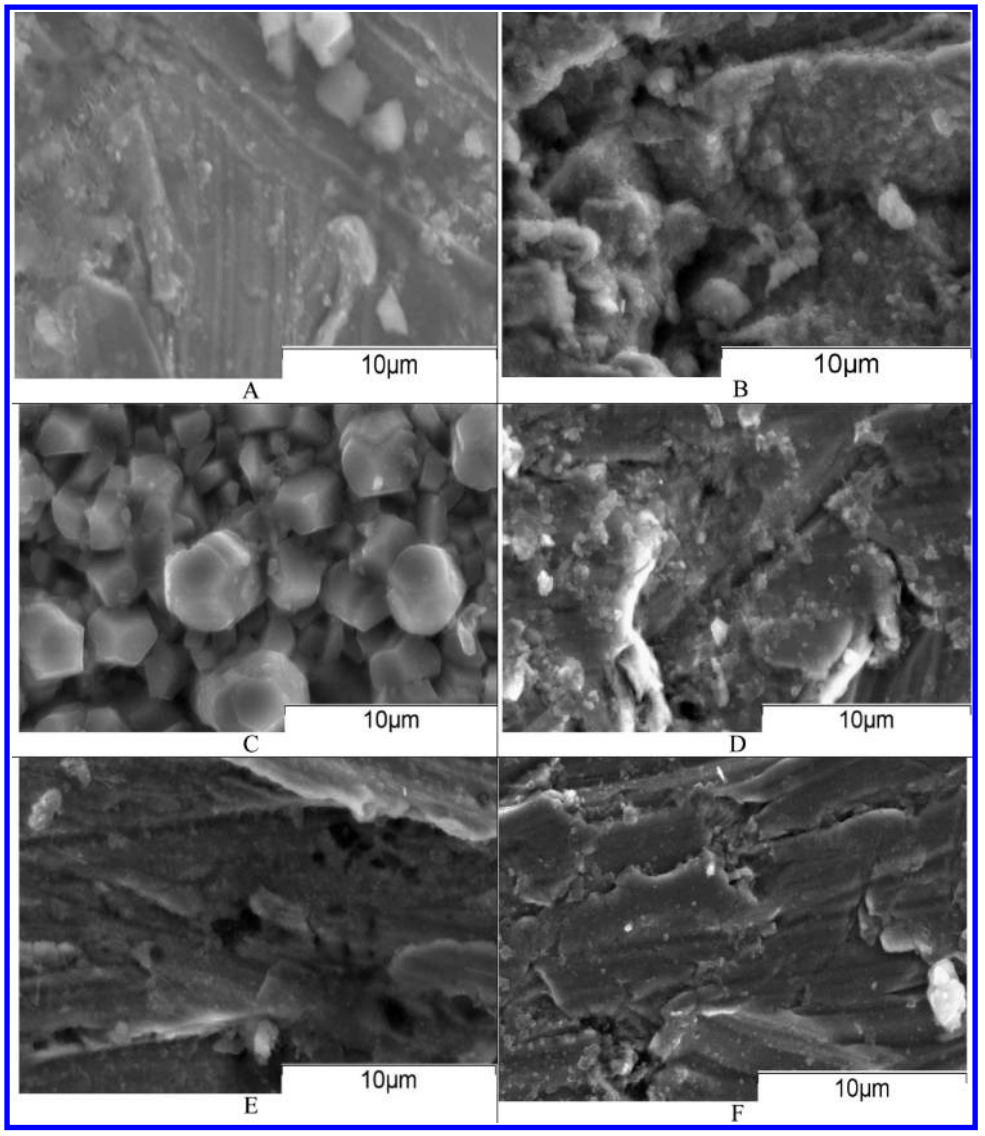

Figure 5. SEM images of the corroded coupons at six positions.

morphologies in Figure 5, part D are similar to those in part B, with the exception of small cracks. Figure 5E,F shows the SEM images of corroded coupons of gas side at the top of absorber and stripper, respectively. The polishing marks can be observed. In Figure 5E, some holes and spiculate corrosion products form on the surface. Some sliced corrosion products and cracks are detected in Figure 5F.

The cross section SEM images of six corroded coupons are shown in Figure 6. The right of all graphs is substrate and left is corroded surface. In Figure 6, parts B and C, there are two layers with different colors, which indicated that the corroded surface contains an inner layer and an outer layer. The corrosion surface between the inner layer and the substrate is relatively uniform compared to that in Figure 6F, which is more locally attacked. This result indicates that the two position corrosion is more serious than others, which is in good agreement with the result of Figure 3.

3.3. EDX Analysis Results. In order to analyze the corroded surface, the EDX was carried out at a scan step of 1 μm. The results are shown in Figures 7 and 8. In Figure 7(a), it can be seen that the scan started from the dark corroded surface, went through the inner phase, and ended at the steel substrate, as indicated by the arrow. Figure 7(b) shows the EDX element profile of the coupon at location B. Three main elements were detected, including carbon, oxygen, and iron. The element hydrogen, however, cannot be detected by EDX so that it is impossible to identify the presence of any hydroxides. The intensity of the carbon signal is high in the outer layer because it is the conductive coating. The level of the oxygen, similar to the iron, is lower than that of the carbon. The inner layer has more oxygen and iron, and less carbon. For steel substrate, the iron count is the highest, and the counts of oxygen and carbon are less than those in the inner layer, but higher than those in the outer layer. This suggests that the primary components of the inner layer are probably iron oxides. The results at other positions are similar except for the position F (shown in Figure 8).

The EDX element profile for location F [Figure 8(b)] is different with that in Figure 7(b), especially for the inner layer. It can be seen that the iron count is slightly more than that of oxygen, and both are much higher than that of carbon. The oxygen content in Figure 8(b) is smaller than that in Figure 7(b). On the contrary, iron is abundant in Figure 8(b). It can be predicted, therefore, that the primary component of the

dx.doi.org/10.1021/ie203045v | Ind. Eng. Chem. Res. 2012, 51, 6714−6721

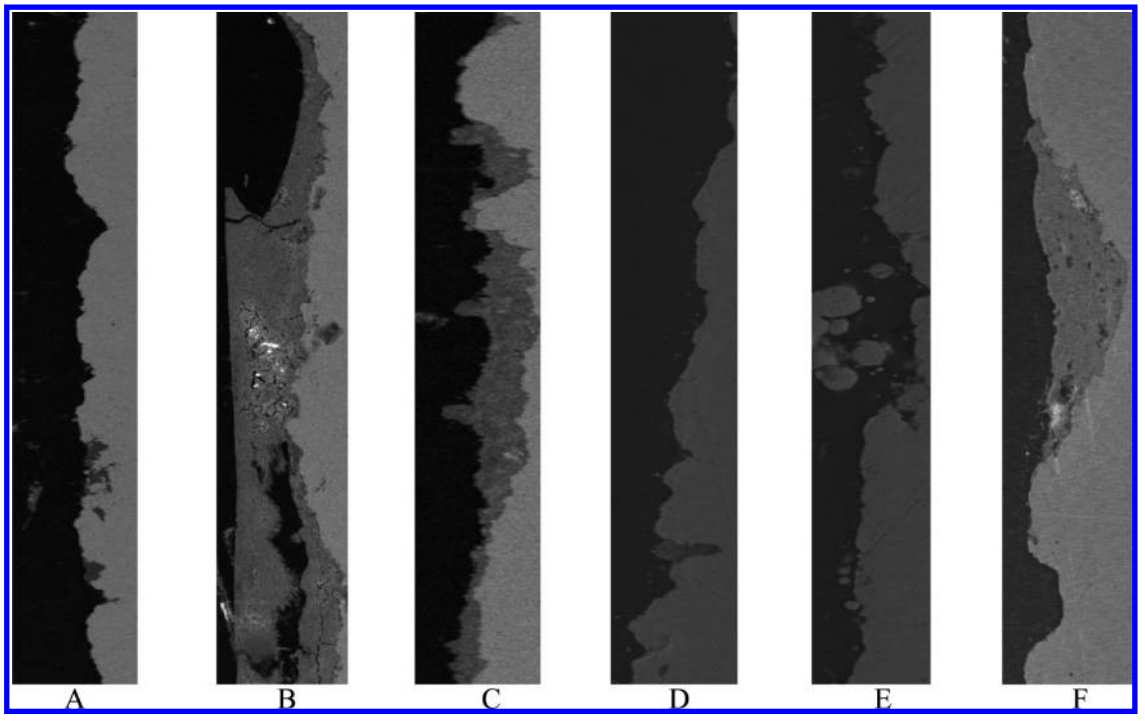

Figure 6. Cross section SEM images of six coupons (200 μm).

inner layer is one of the iron oxides different with that in Figure 7(b). Note that the sulfur element was also observed in Figure 8(b) but never found at other locations.

3.4. XRD and Raman Spectra Analysis Results. To identify the corrosion products mentioned above, further analysis was carried out with XRD and Raman spectroscopy, and the diffraction data analysis software JADE5.0 was utilized. Figure 9 shows the XRD spectra on the corroded coupon surface at location C, in which the siderite ($FeCO_3$) and iron were obtained. This indicates that the dominant corrosion products of the corroded surface are $FeCO_3$, which is the usual product in the CO_2 corrosion environment.[19,20] The weak signals of $FeCO_3$ were also detected at four other locations, with the exception of location A.[21] The iron was also apparently observed on the corroded surface at all locations, especially at location A.[21] It indicates that position C presents more serious corrosiveness than others, which agrees with the results shown in Figure 3.

Figure 10 shows the Raman spectra of the inner layer compounds on the cross sectional surface at locations B and C. No apparent peak was detected at other locations. The strongest Raman peak was observed at 663 cm^{-1}, which, together with the weak peak at 613 cm^{-1}, can be used to identify the corrosion product of magnetite (Fe_3O_4).[22] At the same time, the strongest modes at 225, 293, and 413 cm^{-1} with weak peak at 500 cm^{-1} correspond to hematite (α-Fe_2O_3).[22−24] The Fe_3O_4 and Fe_2O_3 have been observed when siderite decomposed at temperatures below 100 °C and being exposed to oxygen in the air, as shown by the following reactions:[25]

$$FeCO_3 \rightarrow FeO + CO_2 \quad (8)$$

After the initial decomposition shown in eq 8, ferrous oxide (FeO) transforms quickly into Fe_2O_3 and Fe_3O_4:

$$4FeO + O_2 \rightarrow 2Fe_2O_3 \quad (9a)$$

$$3FeO + CO_2 \rightarrow Fe_3O_4 + CO \quad (9b)$$

$$3FeO + H_2O \rightarrow Fe_3O_4 + H_2 \quad (9c)$$

In effect, it is easy to produce passive films from $FeCO_3$ precipitate at locations B and C with high CO_2 loading. According to the above all-analysis results, $FeCO_3$ may decompose as eq 8, and then transform into α-Fe_2O_3 and Fe_3O_4 in the amine aqueous solutions.

The Raman spectra differ from Figure 10 for three locations (B, C, and F), as shown in Figure 11. For parts B and C, Raman spectra were conducted at a small area between the gray layer and the white substrate. The strong modes were observed here at 299 and 385 cm^{-1}, together with another weak peak at 479, 560, and 685 cm^{-1}, could be attributed to α-FeOOH.[22,26,27] α-FeOOH may be transformed from Fe_3O_4.[12] As can be seen from the analysis, the $FeCO_3$ was formed obviously under the condition of high CO_2 loading, and then slowly decomposed and converted to α-Fe_2O_3, Fe_3O_4, and α-FeOOH. Note that the usual corrosion products in the presence of SO_2, ferrous sulfate ($FeSO_4$), and ferrous sulfite ($FeSO_3$),[28] were not observed.

3.5. Contribution of SO_2. Although the sulfur element was detected at the location F, the contribution of SO_2 to corrosion rate is still implicit according to the above analysis. SO_2 was absorbed by amine solutions as follows:

$$SO_2 + H_2O + 2RNH_2 \rightarrow 2RNH_3^+ + SO_3^{2-} \quad (10)$$

The formation of sulfate:

$$2SO_3^{2-} + O_2 \rightarrow 2SO_4^{2-} \quad (11)$$

A reduction of pH with the gradually absorption of SO_2 as time is also shown in Figure 4. Therefore, the absorption of SO_2 also accelerates the cathodic reaction by increasing the amount of H^+ in eq 4. Kladkaew also obtained the same result that a large amount of hydrogen ions will induce a higher corrosion rate.[11] Meanwhile, the oxygen consumption in the presence of 214 ppm SO_2 is higher than that without SO_2. O_2

dx.doi.org/10.1021/ie203045v | Ind. Eng. Chem. Res. 2012, 51, 6714−6721

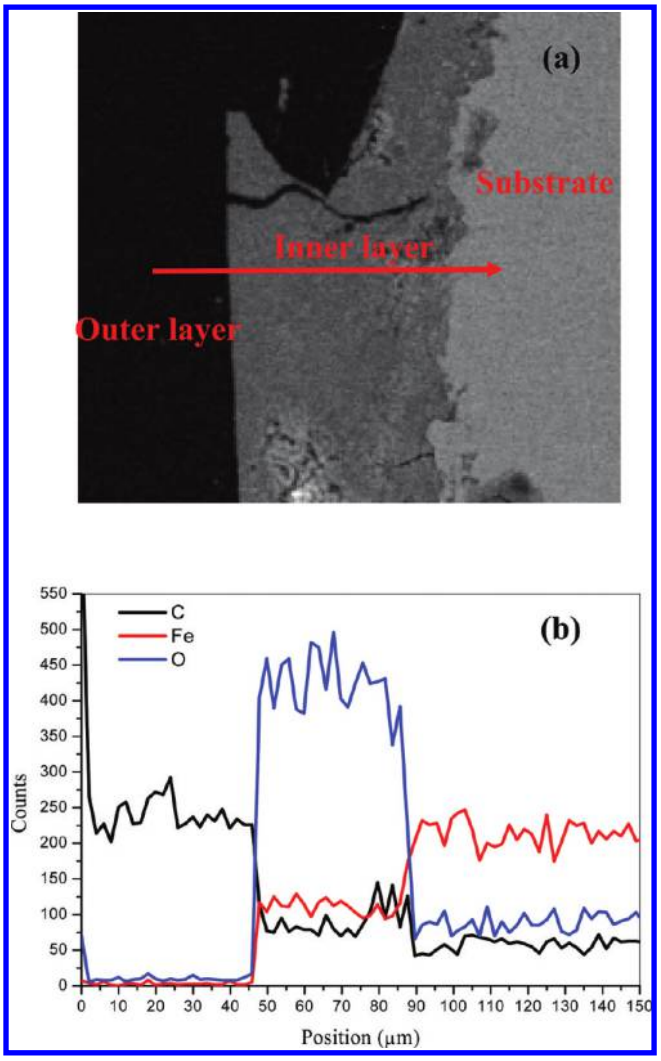

Figure 7. SEM and EDX at location B (a) SEM image (b) EDX element profile.

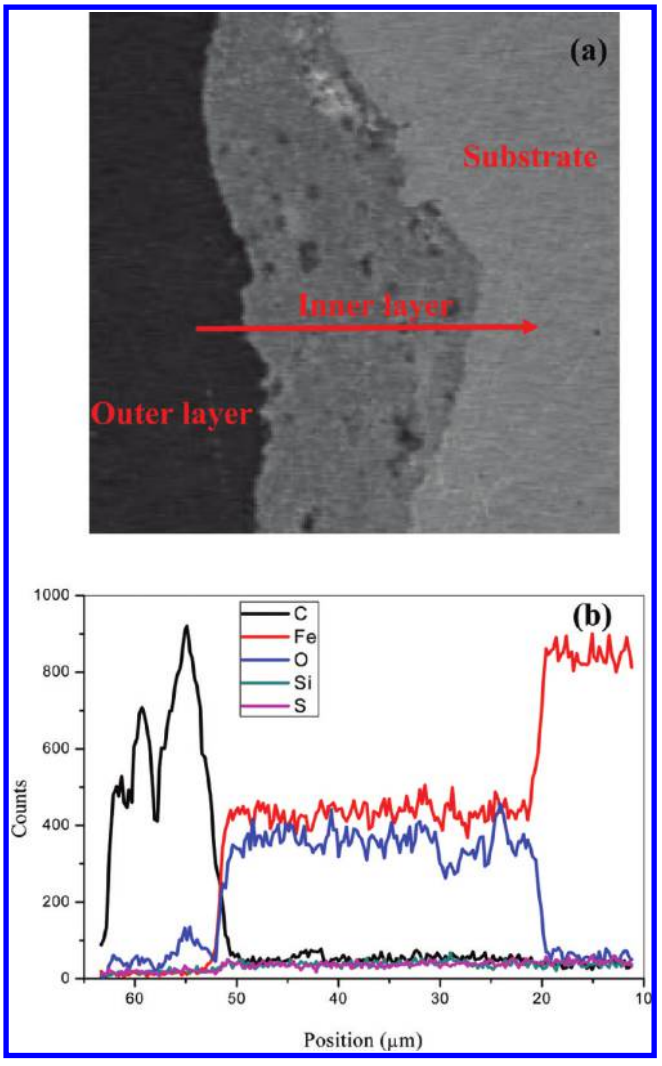

Figure 8. SEM and EDX at location F (a) SEM image (b) EDX element profile.

consumption is around 4% and 0.5% per 12 h, respectively. The higher oxygen consumption by reaction 11 (see Figure 12) may also accelerate the cathodic reaction, in turn, induce a higher corrosion rate as shown in reaction 6.

Kladkaew pointed out that a larger amount of dissolved oxygen in the liquid phase will induce a higher corrosion rate.[11] Moreover, the higher oxygen consumption may accelerate the decomposition of $FeCO_3$.[28] These results confirmed the above analysis on the influence of SO_2 on corrosiveness.

4. CONCLUSIONS

A pilot plant with an amine-based chemical absorption process was continuously operated for about 400 h under the conditions of 12 vol % CO_2, 18 vol %O_2, and 214 ppm SO_2. The corrosion test of carbon steel at six typical locations, including lean liquid inlet of absorber, absorber bottom, rich liquid outlet of rich-lean heat exchanger, stripper bottom, top of absorber, and top of stripper, was conducted. The weight-loss method was used to determine the corrosion rate, XRD, EDX, SEM, and Raman spectroscopy were used to determine the structure of the passive layers and confirm the corrosion products. All test results are summarized below.

The carbon steel at the absorber bottom and rich liquid outlet of the rich-lean heat exchanger shows a higher corrosion rate. The two-layer structure on the corroded cross section was obviously detected at the two positions with high corrosiveness. The corrosion products of the inner layer with gray color are mainly composed of hematite (α-Fe_2O_3) and magnetite

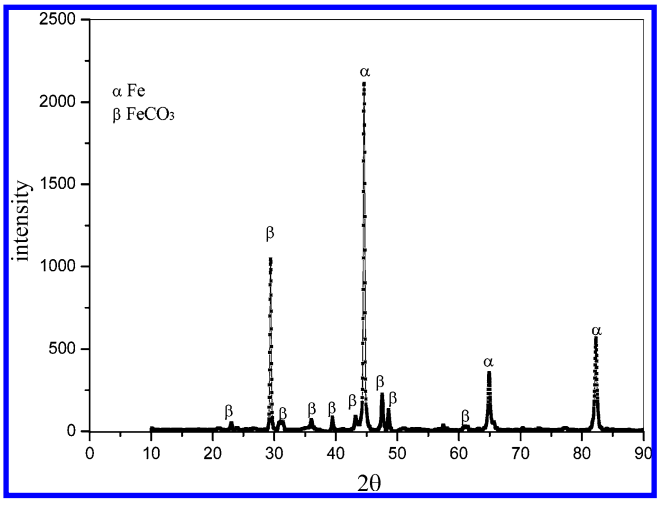

Figure 9. XRD spectra at location C.

dx.doi.org/10.1021/ie203045v | Ind. Eng. Chem. Res. 2012, 51, 6714−6721

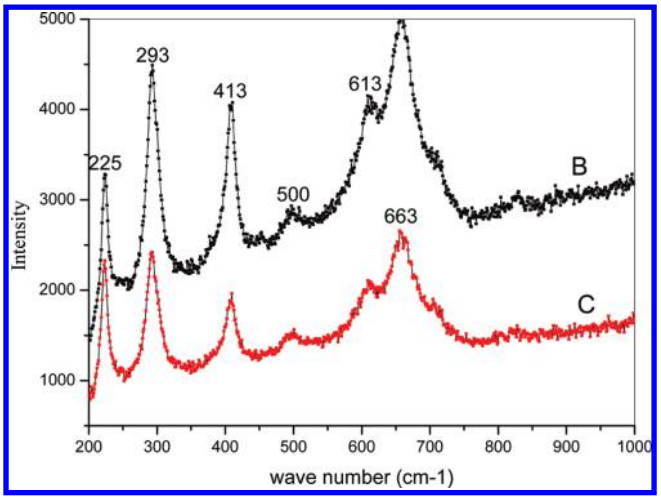

Figure 10. Raman spectra of inner layer at locations B and C.

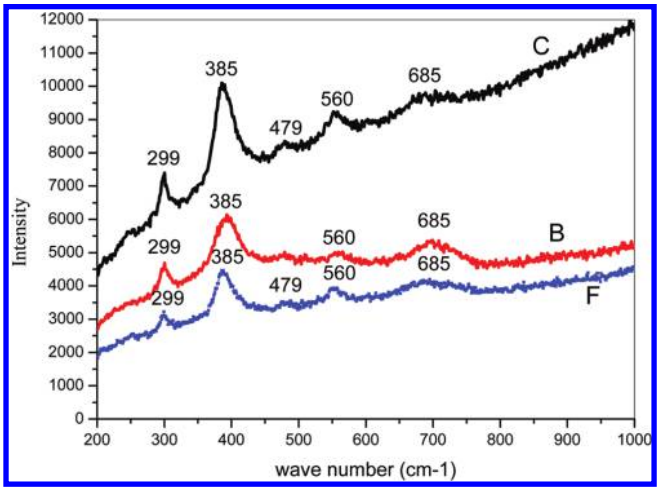

Figure 11. Raman spectra of the inner layer at positions B, C, and F.

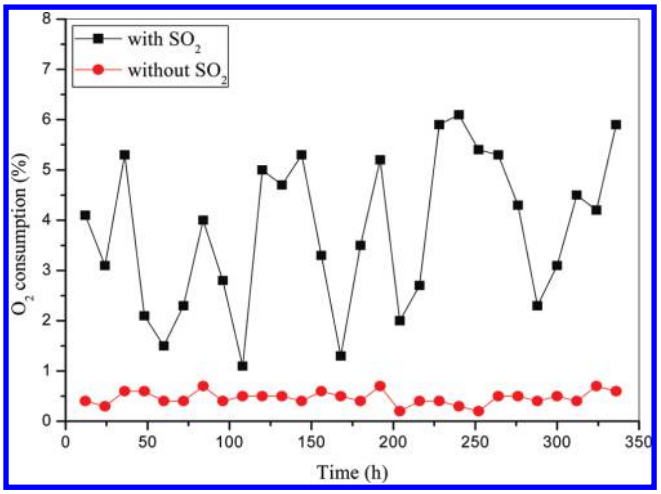

Figure 12. O_2 consumption.

(Fe_3O_4) with trace of goethite (α-FeOOH), whereas the outer layer with dark color is siderite ($FeCO_3$). $FeCO_3$ may slowly decompose, and convert to the magnetite (Fe_3O_4), hematite (α-Fe_2O_3), and goethite (α-FeOOH) in amine aqueous solutions with high CO_2 loading. The addition of SO_2 induces the increase of oxygen consumption and reduction of pH, which may accelerate the corrosion of carbon steel by promoting the cathodic reactions and destroying the passive film of siderite.

AUTHOR INFORMATION

Corresponding Author

*E-mail: gaojb08@mails.tsinghua.edu.cn.

Notes

The authors declare no competing financial interest.

ACKNOWLEDGMENTS

This work was partially supported by TOSHIBA. The authors also would like to thank Sun Ye from Kentucky University for supplying an SEM/EDX test.

NOMENCLATURE

AMP = A sterically hindered amine, 2-amino-2-methy-1-propanol
MEA = Monoethanolamine
MDEA = Methyldiethanolamine
PTFE = Polytetrafluoroethylene

REFERENCES

(1) Ddsideri, U; Paolucci, A. Performance Modelling of a Carbon Dioxide Removal System for Power Plants. *Energy Conversion Manage.* **1999**, *40*, 1899−1915.

(2) Rochelle, G. T. Amine Scrubbing for CO_2 Capture. *Science* **2009**, *325*, 1652−1654.

(3) DuPart M. S.; Bacon T. R.; Edwards D. J. Part2-Understanding Corrosion in Alkanolamine Gas Treating Plants. *Hydrocarbon Process.* **1993**, May, 89−94.

(4) Veawab, A.; Tontiwachwuthikul, P.; Chakma, A. Influence of Process Parameters on Corrosion Behavior in a Sterically Hindered Amine-CO_2 System. *Ind. Eng. Chem. Res.* **1999**, *38* (1), 310−315.

(5) Veawab, A.; Tontiwachwuthikul, P.; Chakma, A. Corrosion Behavior of Carbon Steel in the CO_2 Absorption Process Using Aqueous Amine Solutions. *Ind. Eng. Chem. Res.* **1999**, *38* (10), 3917−3924.

(6) Tanthapanichakoon, W.; Veawab, A. Electrochemical Investigation on the Effect of Heat-Stable Salts on Corrosion in CO_2 Capture Plants Using Aqueous Solution of MEA. *Ind. Eng. Chem. Res.* **2006**, *45* (8), 2586−2593.

(7) Soosaiprakasam, I. R.; Veawab, A. Corrosion and Polarization Behavior of Carbon Steel in MEA-Based CO_2 Capture Process. *Int. J. Greenhouse Gas Control* **2008**, *2* (4), 553−562.

(8) Nainar, M; Veawab, A. Corrosion in CO_2 Capture Process Using Blended Monoethanolamine and Piperazine. *Ind. Eng. Chem. Res.* **2009**, *48* (20), 9299−9306.

(9) Veawab, A; Tontiwachwuthikul, P; Bhole, S. D. Studies of Corrosion and Corrosion Control in a CO_2-2-Amino-2-methyl-1-propanol (AMP) Environment. *Ind. Eng. Chem. Res.* **1997**, *36* (1), 264−269.

(10) Veawab, A; Tontiwachwuthikul, P; Chakma, A. Investigation of Low-Toxic Organic Corrosion Inhibitors for CO_2 Separation Process Using Aqueous MEA Solvent. *Ind. Eng. Chem. Res.* **2001**, *40* (22), 4771−4777.

(11) Kladkaew, N; Idem, R; Tontiwachwuthikul, P; Saiwan, C. Corrosion Behavior of Carbon Steel in the Monoethanolamine−H_2O−CO_2−O_2−SO_2 System. *Ind. Eng. Chem. Res.* **2009**, *48* (19), 8913−8919.

(12) Guo, X. P.; Tomoe, Y. The Effect of Corrosion Product Layers on the Anodic and Cathodic Reactions of Carbon Steel in CO_2-Saturated MDEA Solutions at 100 °C. *Corros. Sci.* **1999**, *41*, 1391−1402.

(13) Kittel, J; Idem, R; Gelowitz, D; et al. Corrosion in MEA Units for CO_2 Capture: Pilot Plant Studies. *Energy Procedia* **2009**, *1*, 791−797.
(14) Gao, J. B.; Wang, S. J.; Zhao, B; Qi, G. J.; Chen, C. H. Pilot-Scale Experimental Study on the CO_2 Capture Process with Existing of SO_2: Degradation, Reaction Rate and Mass Transfer. *Energy Fuels* **2011**, *25* (12), 5802−5809.
(15) Gao, J. B.; Wang, S. J.; Zhou, S; Zhao, B; Chen, C. H. Corrosion and Degradation Performance of Novel Absorbent for CO_2 Capture in Pilot-Scale. *Energy Procedia* **2011**, *4*, 1534−1541.
(16) Gao, J. B.; Wang, S. J.; Zhou, S; Zhao, B; Chen, C. H. Experimental Study on the Influence of SO_2 to the CO_2 Capture Process. *Proc. CSEE* **2011**, *31* (5), 52−57.
(17) Nesic, S.; Postlethwaite, J.; Olsen, S. An Electrochemical Model for Prediction of Corrosion of Mild Steel in Aqueous Carbon Dioxide Solutions. *Corrosion* **1996**, *54* (4), 280.
(18) Zheng, D. H.; Che, D. F.; Liu, Y. H. Experimental Investigation on Gas−Liquid Two-Phase Slug Flow Enhanced Carbon Dioxide Corrosion in Vertical Upward Pipeline. *Corros. Sci.* **2008**, *50*, 3005−3020.
(19) Han, J. B.; Young, D; Colijn, H; Tripathi, A; Nešić, S. Chemistry and Structure of the Passive Film on Mild Steel in CO_2 Corrosion Environments. *Ind. Eng. Chem. Res.* **2009**, *48*, 6296−6302.
(20) Heuer, J. K.; Stubbins, J. F. An XPS Characterization of $FeCO_3$ Films from CO_2 Corrosion. *Corros. Sci.* **1999**, *41*, 1231−1243.
(21) Gao, J. B.; Wang, S. J.; Zhao, B; Chen, C. H. Absorber Corrosion Performance for CO_2 Capture Using an Amine Absorbant in a Coal-Fired Power Plant. *J. Tsinghua Univ. (Sci. & Tech.)* **2011**, *51* (5), 657−661.
(22) Thibeau, R. J.; Brown, C. W.; Heidersbach, R. H. Raman-Spectra of Possible Corrosion Products of Iron. *Appl. Spectrosc.* **1978**, *32* (6), 532−535.
(23) Ohtsuka, T; Kubo, K; Sato, N. Raman-Spectroscopy of Thin Corrosion Films on Iron at 100°C to 150°C in Air. *Corrosion* **1986**, *42* (8), 476−481.
(24) Beattie, I. R.; Gilson, T. R. Single-Crystal Raman Spectra of Nearly Opaque Materials-Iron (III) Oxide and Chromium (III) Oxide. *J. Chem. Soc. A* **1970**, *6*, 980.
(25) Heuer, J. K.; Stubbins, J. F. An XPS Characterization of $FeCO_3$ Films from CO_2 Corrosion. *Corros. Sci.* **1999**, *41* (7), 1231−1243.
(26) Nauer, G; Strecha, P; Brinda-Konopik, N; Lipstay, G. Spectroscopic and Thermoanalytical Characterization of Standard Substances for the Identification of Reaction-Products on Iron Electrodes. *J. Therm. Anal.* **1985**, *30* (4), 813−830.
(27) Thierry, D; Persson, D; Leygraf, C; Boucherit, N; Hugot-Le Goff, A. Raman-Spectroscopy and XPS Investigations of Anodic Corrosion Films Formed on Fe−Mo Alloys in Alkaline-Solutions. *Corros. Sci.* **1991**, *32* (3), 273−284.
(28) Choi, Y; Nesic, S; Young, D. Effect of Impurities on the Corrosion Behavior of CO_2 Transmission Pipeline Steel in Supercritical CO_2-Water Environments. *Environ. Sci. Technol.* **2010**, *44* (23), 9233−9238.